Philosophical Magazine,
Vol. 85, Nos. 4–7, 01 February–01 March 2005, 779–797

Taylor & Francis
Taylor & Francis Group

On the effect of dose rate on irradiation hardening of RPV steels

G.R. ODETTE*, T. YAMAMOTO and D. KLINGENSMITH

Department of Mechanical and Environmental Engineering and
Department of Materials, University of California Santa Barbara,
Santa Barbara, CA 93106, USA

The effect of dose rate (DR), or neutron flux (ϕ), on irradiation hardening ($\Delta\sigma_y$) and embrittlement of reactor pressure vessel (RPV) steels is a key unresolved issue. We report a rigorous evaluation of DR effects based on a very large $\Delta\sigma_y$ database we developed for RPV steels with a wide range of compositions, including a set of split-melt alloys with controlled and systematic variation in Cu, Ni and Mn content. The steels were irradiated at 290°C in three ϕ-regimes to a wide range of overlapping fluences (ϕt). The contribution of copper-rich precipitates (CRPs) to $\Delta\sigma_y$ increases up to a plateau hardening that is a strong function of the alloy Cu, Ni and Mn content, but is relatively independent of DR. However, the pre-plateau region is shifted to higher ϕt with increasing DR. The shift can be approximately accounted for by defining an effective fluence (ϕt_e) as $\phi t_e \approx \phi t(\phi_r/\phi)^{1/2}$, where ϕ_r is a reference flux. The $\phi^{-1/2}$ scaling is consistent with a vacancy plus self-interstitial-atom (SIA) recombination rate controlling mechanism. The $\Delta\sigma_y$ data are analysed with a combined model describing: (a) the excess vacancy concentration under irradiation as a function of DR, including the effect of solute vacancy traps on recombination; (b) the corresponding radiation enhanced Cu diffusion (RED) coefficient (D*); (c) the resulting accelerated growth of CRPs; and (d) the contribution of CRPs to $\Delta\sigma_y$. Recombination is shown to increase with higher alloy Ni and Mn content, consistent with a solute–vacancy trapping mechanism. In spite of high recombination rates, however, RED is extremely efficient, with the D* ranging up to a factor of 60 or more times higher than predicted by simple rate theory models. Various explanations of the high diffusion rates are discussed, including large vacancy–solute binding energies that control the vacancy concentrations and jump frequencies near solutes in a way that can enhance both diffusion and recombination.

1. Introduction

In service, exposure to energetic neutrons degrades the fracture toughness of reactor pressure vessel (RPV) steels. Irradiation embrittlement is typically characterized by an increase in a temperature (ΔT) marking the transition between the low toughness

*Corresponding author. Email: odette@engineering.ucsb.edu

Philosophical Magazine
ISSN 1478–6435 print/ISSN 1478–6443 online
http://www.tandf.co.uk/journals
DOI: 10.1080/14786430412331319910

cleavage and high toughness ductile fracture regimes. A large number of irradiation and metallurgical variables, and *variable combinations*, control ΔT[1–5]. Irradiation variables include the neutron flux (ϕ), fluence (ϕt) and spectrum and temperature (T_i). The metallurgical variables include the start-of-life concentrations and distributions of solutes (like Cu, Ni, Mn and P) and the microstructure that are mediated by both the alloy's composition and thermo-mechanical processing history. Fundamental research has provided improved understanding of embrittlement, leading to physically based models that have increased the reliability of statistical ΔT data correlations [2, 3, 6–9].

However, proper treatment of ϕ, or dose rate (DR) effects is a key outstanding issue [10]. The primary mechanism of embrittlement in RPV steels is irradiation hardening ($\Delta\sigma_y$) produced by nm-scale features that develop under irradiation [1–3, 6–9]. The sequence of relations — ΔT to $\Delta\sigma_y$ – nanofeatures to $\Delta\sigma_y$ – irradiation and metallurgical variables to the nanofeatures — can be linked in hierarchical multiscale models [8]. Both the effects of the nanofeatures on $\Delta\sigma_y$ and $\Delta\sigma_y$ on ΔT have been developed and continue to be refined. The focus of this work is on the effect of DR on the kinetics of the evolutions of nanofeatures themselves. These include matrix features (MFs), believed to be solute–vacancy cluster complexes, and Cu-rich precipitates (CRPs). The MFs form in aged displacement cascades and dissolve by vacancy emission over characteristic annealing times [3, 11–13]. Sub nm-scale cluster complexes that dissolve over periods that are much less than typical test reactor irradiation times are called unstable matrix features (UMFs); and slightly larger cluster complexes that persist for much longer times are called stable matrix features (SMFs). The MFs contain a variety of solutes that bind to the vacancies, including Ni and Mn; but MFs do not require Cu to form.

Dissolved Cu is highly supersaturated at typical impurity levels ($>\approx 0.1$ wt%) and it diffuses and clusters to form a high density of nm-scale coherent CRPs alloyed with Mn and Ni [3, 6, 12]. Copper precipitation is relatively slow under thermal ageing conditions at PRV operating temperatures around 290°C, but is greatly accelerated by radiation-enhanced diffusion (RED). Enhanced diffusion results from an excess concentration of migrating vacancies that are generated by atomic displacements in cascades created by the high-energy recoils from neutron–nuclear interactions. Other fine scale features that form under irradiation, in some circumstances, include self-interstitial atom (SIA) cluster-dislocation loops as well as alloy carbides, nitrides and phosphides and Mn–Ni–Si rich precipitates [3, 12]. The thermodynamics and kinetics of the nanofeature evolutions are mediated by the combination of irradiation and metallurgical variables, hence, intrinsically depend on both T_i and ϕ.

Two-feature, CRP plus SMF models, such as the one described in NUREG/CR 6551, form the current basis for predicting RPV embrittlement [2]. In the NUREG study, physically based, analytical models were fitted to a large power reactor engineering database of 609 ΔT data points from reactor surveillance programmes. The CRP contribution to ΔT is a product of two terms: one depends on the alloy Cu and Ni content; and the other is a function of ϕ and ϕt. The CRP contribution to embrittlement saturates at high ϕt due to Cu depletion, at a ΔT that is independent of DR. Higher DR shifts the pre-plateau CRP contribution to higher ϕt. The SMF is independent of Cu and DR, but increases with increasing P and decreasing T_i. The SMF contribution does not saturate, increasing roughly in proportion to $\sqrt{\phi t}$. The NUREG model is schematically illustrated in figure 1a. Here $\Delta\sigma_{ypm}$ is the maximum

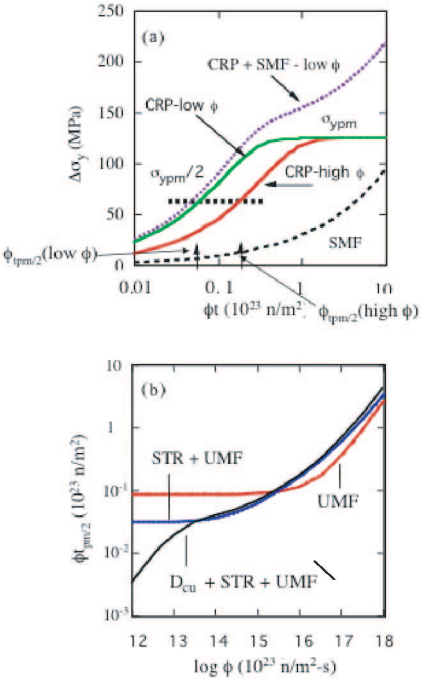

Figure 1. (a) Schematic illustration of the CRP plus SMF model of irradiation hardening. Note the ϕt needed to produce 50% of the maximum CRP hardening is indicated as $\phi t_{pm/2}$ and increases with increasing ϕ. (b) A schematic illustration of the DR dependence for various combinations of thermal diffusion contributions to D* (D_{cu}), solute trap recombination (STR) and unstable matrix feature (UMF) sink mechanisms. The STR mechanism is the dominant in the intermediate DR regime that is the focus of this study.

precipitate contribution ($\Delta\sigma_{yp}$) to $\Delta\sigma_y$. The ϕt needed to reach $\Delta\sigma_{ypm}/2$ is specified by $\phi t_{pm/2}$. Note, $\phi t_{pm/2}$ increases with increasing DR. Similar two-feature models developed by various British researchers have long been the basis for predicting ΔT for both C–Mn–Ni–Mo light water reactor (LWR)-type steels [9] and C–Mn steels used in Magnox reactors [7].

The NUREG analysis found a DR dependent embrittlement regime at very low ϕ, less than about $10^{14}\,nm^{-2}\,s^{-1}$. This DR effect is likely caused by the anomalous rapid thermal diffusion of Cu, leading to precipitation, and corresponding age hardening, that would, in the limit, occur even in the absence of irradiation. Strong evidence in support of this hypotheses is found in thermal age hardening due to Cu precipitation observed in Fe–Cu–Mn model alloys, as well as high Ni and Cu RPV steels. Ageing at 290 and 350°C for periods of only 7200 h resulted in $\Delta\sigma_y$ up to 185 MPa [14]. Both 3-D atom probe [15] and combined electrical resistivity and Seebeck coefficient measurements [16] have shown that the amount of thermal Cu precipitation is consistent with measured $\Delta\sigma_y$. There is also substantial evidence for DR effects at high ϕ, characteristic of greatly accelerated test reactor irradiations [3, 11, 12].

The balance between the vacancy generation rate and the corresponding net rate at which they annihilate at sinks and recombine with SIA governs the RED rates. A DR-dependent regime is believed to begin above about $5 \times 10^{15}\,nm^{-2}\,s^{-1}$ at 290°C

due to a high concentration of the UMF clusters generated in aged displacement cascades that act as sinks for mobile defects [3, 11, 12]. The UMF sinks eliminate equal fluxes of vacancies and SIA (effectively recombining them), thus slowing the RED growth of CRPs by lowering D*. The presence of such vacancy cluster-complexes (nanovoids) has been demonstrated in model alloys by both small angle neutron scattering (SANS) and positron annihilation (PAS) studies [17, 18]. In more complex alloys, solutes like Mn, Ni, P, Si, C and N are also likely to segregate to smaller, but more numerous UMF cluster-complexes. Low-temperature (290 and 350°C) post-irradiation annealing has been used to characterize the UMFs [3, 11, 19].

The net Cu diffusion leading to a given amount of precipitation at a specified ϕt, is $D^*t = D^*\phi t/\phi$, where D* is the RED coefficient. Thus if D* scales with ϕ^p, then $\phi t_{pym}/2$ scales with ϕ^{1-p}. In the UMF sink-dominated regime, D* has a T_i-dependent maximum value that is independent of $\phi (p = 0)$. In this case, $D^*\phi t/\phi$ depends only on the irradiation time (t_i) and T_i, thus $\phi t_{pym}/2$ scales with ϕ [3, 11, 12]. At lower DR, $D^* \alpha \phi^p$, where $p < 1$ due to UMF sinks and SIA–vacancy recombination. In the recombination dominated regime, D* increases with $\phi^{1/2}$ $(p = 1/2)$ and the corresponding $\phi t_{pym}/2$ scales with $\phi^{1/2}$ and depends on T_i [3, 12]. Recombination can be neglected in pure iron at DRs even well in excess of those typically encountered in accelerated RPV steel test reactor irradiations [5, 12]. However, in alloys, solutes bind with and trap vacancies [20], thereby increasing recombination rates. Strong solute vacancy trapping shifts the recombination dominated DR regime down to much lower ϕ.

Network dislocations are the primary fixed defect sinks. Recombination becomes negligible at low DRs in the dislocation sink dominated regime. In this case, D* increases in proportion to DR, as $D^* \alpha \phi$ $(p = 1)$, thus $\phi t_{pym}/2$ is independent of DR and T_i. However, as noted above, the thermal diffusion coefficient (D_{cu}) of Cu may approach D* at very low DR. In the limiting case, where $D^* \approx D_{cu}$, the $D^*\phi t/\phi$ is again only a function of t_i and $\phi t_{pym}/2$ scales with ϕ and depends on T_i. The magnitudes of D_{cu} and D* depend on complex binding interactions between vacancies and solutes that increase the thermal vacancy concentration and control the frequencies of five (or more) vacancy exchanges with the solute and neighbouring (primarily Fe) atoms [21–23]. Solute–vacancy binding leads to a D_{cu} that is significantly greater than the self-diffusion coefficient (D_{sd}) [21–23] and thus a correspondingly larger D*.

In summary, DR effects are expected to occur over a wide range of ϕ due to the combination of: (a) thermal contributions to Cu diffusion (D_{cu}) at very low DRs; (b) solute trap enhanced recombination (STR) over a range of intermediate DRs; and (c) UMF sinks at the highest DRs. Indeed, DR independence is expected only for fixed (dislocation) sink-dominated conditions lying between the thermal diffusion and recombination-dominated regimes. This is schematically illustrated in the plot of $\phi t_{pm/2}$versus ϕ in figure 1b for various combinations of mechanisms. Extensive test reactor studies by Williams and co-workers have shown a strong DR dependence in the intermediate ϕ regime [9]. However, this database is primarily for relatively low $T_i \approx 260$°C. The actual scaling laws governing DR effects and boundaries of the various regimes at ≈ 290°C are not well established. This is particularly true in the critical low-to-intermediate DR regime, from about ≈ 0.05 to $5 \times 10^{15}\,nm^{-2}\,s^{-1}$, encompassing typical surveillance and vessel environments in pressurized water reactors (PWRs).

In the remainder of this paper we focus on a rigorous evaluation of DR effects based on irradiation of a large number of RPV steels in the University of California Santa Barbara (UCSB) Irradiation Variable (IVAR) facility located at the University of Michigan Ford Research Reactor (FRR). The irradiations analysed here were carried out at 290°C in three different ϕ regimes, from $\approx 6 \times 10^{14}$ to $9 \times 10^{15}\,\mathrm{nm^{-2}\,s^{-1}}$, over a range of overlapping ϕt (4 to 8 in each ϕ regime) from $\approx$0.04 to $4 \times 10^{23}\,\mathrm{nm^{-2}}$. The alloy matrix included a total of 44 RPV steels, 35 with $\geq$0.1% Cu and 9 with low or no Cu. The alloy matrix included both split-melt heats with a wide range of controlled variations in Cu, Ni and Mn contents, as well as a number of commercial type welds and some base metals. The overall database consists of 647 irradiation and material conditions. Post irradiation studies included both tensile tests to measure $\Delta\sigma_y$ and small-angle neutron scattering (SANS) characterization of the embrittlement nanostructures. In this paper the $\Delta\sigma_y$ data are analysed using standard rate theory models. Details of the analysis of the SANS data will be reported in a future paper.

2. Experimental

2.1. *Alloys*

The alloys investigated in this study were characterized by optical metallography, as well as baseline tensile and hardness testing. Compositions (reported here in wt%) were determined by a combination of atomic absorption spectroscopy and interstitial element analysis. For simplicity and consistency, we use nominal compositions in this paper. A detailed compilation of the actual alloy compositions, processing paths and heat treatments can be found elsewhere [1, 4]. The alloys are classified in two broad groups:

1. CM-series and L-series: A set of 27 complex A533B-type split-melt bainitic steels with single-variable composition variants to evaluate the effects of different combinations of Cu (0.0–0.8%), Ni (0.0–1.6%), Mn (0–1.6%) and P (0.005–0.040%). These alloys had typical prior austenite grain sizes of $\approx$ 50 μm and microstructures ranging from tempered bainite to mixed tempered bainite-ferrite. The unirradiated σ_y varied from about 385 to 500MPa, averaging $\approx$ 470 MPa.
2. CWP-series: A set of 17 commercial-type, reference or program welds and base metals. There is a significant database on both unirradiated and irradiated tensile properties on most of these steels. The CWP-series consists of: 10 intermediate $\approx$ 0.6–0.8% Ni submerged arc welds (SAW) with 0.06–0.35% Cu; 3 high $\approx$ 1.6% Ni SAW with 0.04–0.55% Cu; and 4 low to intermediate $\approx$ 0.2–0.8% Ni base metals with $\leq \approx$ 0.14% Cu. The CWP-series encompassed a wide range of prototypic tempered bainitic-ferritic low alloy steel microstructures with unirradiated σ_y that varied from about 425 to 550 MPa, averaging $\approx$ 500 MPa.

2.2. *Specimens, irradiations and post-irradiation testing*

Sub-sized sheet tensile specimens with a 9 mm long by 5 mm wide gauge section were precision punched from lapped 0.5-mm coupons. Two or more tests were carried

out for each alloy-irradiation condition on a screw driven load frame at a strain rate of $5.6 \times 10^{-2}\,s^{-1}$. The average 1 SD-uncertainty in σ_y ($\delta\sigma_y$) was about ± 15 MPa. In cases where there are only two tests, $\delta\sigma_y$ was assumed to be the deviations from the mean. The corresponding uncertainties in $\Delta\sigma_y$ were taken as the root mean square of the individual $\delta\sigma_y$ for the irradiated and unirradiated tests. Additional details of the tensile testing are given elsewhere [4].

The irradiations were carried out at the IVAR facility at the FRR. Oak Ridge National Laboratory (ORNL) operated IVAR for the US Nuclear Regulatory Commission (NRC) sponsored program at UCSB. The facility was designed by UCSB and ORNL to provide irradiations at up to three well-controlled T_i in three DR regimes defined as: low $\phi \approx 0.9 \pm 0.3 \times 10^{15}\,nm^{-2}\,s^{-1}$; intermediate $\phi \approx 3 \pm 0.5 \times 10^{15}\,nm^{-2}\,s^{-1}$; and high $\phi \approx 8 \pm 3 \times 10^{15}\,nm^{-2}\,s^{-1}$. Here, the ϕ and ϕt are for neutron energies greater than 1 MeV. The specimens were contained in small capsules that could be inserted or removed at the end of a 12-day reactor cycle, thus providing the opportunity to easily obtain multiple increments of ϕt; the number of increments and ϕt-range depended on the alloy and DR. At high ϕ there were 7 to 8 ϕt increments from ≈ 0.04 to $3.3 \times 10^{23}\,nm^{-2}$; at intermediate ϕ there were 6 ϕt increments from ≈ 0.04 to $1.6 \times 10^{23}\,nm^{-2}$; and at low ϕ there were 4 to 8 ϕt increments from 0.006 to $0.4 \times 10^{23}\,nm^{-2}$. The actual ϕ and ϕt for the 17 290°C IVAR capsules that are the source of data for this paper were based on detailed ϕ maps provided ORNL [24] and are reported elsewhere [5]. We also independently evaluated the ϕ at various locations based on activation measurements of Fe and Ni monitor wires included in a subset of the capsules. The ϕ and ϕt values are estimated to be accurate within about $\pm 10\%$. Irradiation temperatures were monitored and controlled by a large number of thermocouples located in close proximity to the specimen capsules. The absolute temperatures of the samples are based on detailed heat transfer calculations and are estimated to be accurate within ± 5°C.

3. A fitting model of DR effect to analyse the IVAR database

The primary purpose of the standard rate theory based $\Delta\sigma_y(\phi t, \phi)$ *fitting* model we develop in this section was to systematically analyse and extract physically relevant parameters from the enormous IVAR database. The model was intended to answer the question: what does the IVAR database reveal about the effects of metallurgical and irradiation variables in general, and about DR effects in particular? The model was fit to each individual alloy irradiated to various ϕt levels at what we term high, intermediate and low DRs. Notably, the model was not intended be a full theoretical predictive treatment of embrittlement. However, the fitting model was structured to reflect the most likely, and we believe robust, set of physical embrittlement mechanisms [3, 12]. The basic validity of the fitting model is reflected by the high degree to which it has been found to be consistent with the observed data trends. Thus the model provides a good physical basis for extracting and interpreting the various fit parameters.

The fitting model framework is as follows. First, we evaluated the steady-state vacancy concentration (atom fraction) X_v as a function of non-dimensional parameters (e.g., η and g_s – see below) representing combinations of the material properties of a particular alloy irradiated at a specified ϕ and T_i. The X_v was then related to the corresponding radiation enhanced diffusion (RED) coefficient (D*).

The D* was next used in a Avrami-type transformation expression (see e.g. [25]) to model the CRP growth kinetics as a function of ϕ and ϕt, in terms of $f_p(\phi t, \phi)/f_{pm}$; here $f_p(\phi t, \phi)$ is the CRP volume fraction at a specified ϕt and ϕ, and f_{pm} is the maximum (or plateau) volume fraction. Finally, a dispersed obstacle hardening relation, $\Delta\sigma_{yp} = \Delta\sigma_{ypm}\sqrt{f_p/f_{pm}}$, was used to model the corresponding CRP contribution ($\Delta\sigma_{yp}$) to $\Delta\sigma_y(\phi t)$, where $\Delta\sigma_{ypm}$ is the maximum, or plateau, hardening.

Defect conservation balances, treating vacancy and SIA production, transport and fate, were used to establish the steady-state $X_v(\phi)$ [3, 12, 26]. If X_v is proportional to ϕ there is no DR effect; if X_v is proportional to ϕ^p, where $p < 1$, then there is a DR effect of the type illustrated in figure 1, where $\phi t_{pm/2}$ scales with ϕ^{1-p}. Vacancy fates include clustering, annihilation at sinks and recombination with SIA. The dominant fixed sinks are dislocations. The UMF also act as sinks that are dominant at very high DRs. The model uses standard expressions for the individual sink strengths [26]: for spherical UMF, as well as isolated vacancies that act as sites for SIA recombination, $S_{c/v} \approx 4\pi N_{c/v} r_{c/v}$, where $N_{c/v}$ and $r_{c/v}$ are the sink number density and capture radius respectively; and for an orderly arrangement of a net density ρ of straight segments, the dislocation sink strength is $S_d \approx \rho$. The total sink strength is $S_t = S_c + S_d$. The model neglects bias, which would have a small effect on X_v and RED. Note in the very low dose regime, pertinent to RPV irradiations, bias driven defect accumulation of voids and dislocation loops is insignificant. However, a growing population of SMFs, that may act as fixed sinks, do develop with increasing ϕt. This effect slows the growth of CRPs at high ϕt, but is effectively accounted for in the Avrami model fitting parameter, β, that is discussed below. The model also assumes that a sink easily absorbs any defect that arrives at its capture radius. Note, the effects of both actual sink efficiency and complex geometric arrangements of dislocation structures that are found in RPV steels may reduce the effective S_d to a value significantly less than ρ. Finally, it is important to note that there is no evidence in the IVAR database of $\phi - T_i$ kinetics that would be associated with so-called production bias rate theory, that assumes a dominant role of one-dimensional diffusion of clusters that contain most of the SIAs [27, 28]. Specifically, the effective sink strength for solute trapped vacancies is much too low for SIA clusters that migrate one-dimensionally to produce the large fraction of defect recombination that is observed in the IVAR database.

Since DR effects are governed by the vacancy concentrations, we first derive a quantitative model of $X_v(\phi)$. The nominal parameters used in the numerical evaluations of $X_v(\phi)$ are shown in parenthesis following the definition of the term. However, it is important to once again emphasize that neither the parameters, nor most of the assumptions described above, affect the use of the model to fit the $\Delta\sigma_y$ database. Rather, the fits yield both non-dimensional and absolute values of the parameters for a particular alloy and irradiation condition that can then be compared to the model predictions to evaluate the validity of both the input parameters and various assumptions in the model.

It is convenient to express X_v in terms of the fraction of vacancies and SIA that escape recombination and reach fixed dislocation sinks (g_s) as,

$$X_v = \frac{[g_s(T, \phi, S_t)\xi\phi\sigma_{dpa}]}{[D_v S_t]} \tag{1a}$$

Here σ_{dpa} ($= 1.5 \times 10^{-25}\,m^2$) is the displacement-per-atom (dpa) cross-section, ξ ($= 0.4$) is the fraction of vacancies and SIA created per dpa, D_v ($1.13 \times$

$10^{-16}\,m^2\,s^{-1}$ at 290°C) is the vacancy diffusion coefficients ($\ll$ than the interstitial diffusion coefficient). If $g_s = 1$ (the sink dominated case) there is no DR effect; if $g_s < 1$ there is a DR effect. For recombination that occurs as vacancies and SIA diffuse freely through the ferrite matrix [12]

$$g_{sm} = \left[\frac{2}{\eta}\right][(1+\eta)^{1/2} - 1], \tag{1b}$$

$$\eta = \frac{16\pi r_v \xi \phi \sigma_{dpa}}{\Omega_a D_v S_t^2} \tag{1c}$$

Here r_v ($=0.57\,nm$) is the SIA-vacancy recombination radius and Ω_a ($=1.17\times10^{-28}\,m^3$) is the atomic volume. Using the nominal parameters and $S_t = S_d = 2\times10^{-14}\,m^2$ (taken as the nominal baseline value) significant recombination, defined by $g_s = 0.5$, occurs at a high DR for $\phi > 3\times10^{17}\,nm^{-2}\,s^{-1}$ at 290°C.

However, recombination is greatly enhanced if vacancies are strongly bound to a high concentration (X_t) of solute trapping sites. Assuming that a solute trap is limited to one bound vacancy and that a small fraction of traps are occupied ($X_t \gg X_{tv}$),

$$\xi\phi\sigma_{dpa} + \frac{X_{tv}}{\tau_t} - D_v X_v\left[\frac{S_t + 4\pi(r_t X_t + r_r X_v)}{\Omega_a}\right] = 0 \tag{2a}$$

$$\frac{D_v X_v 4\pi r_t X_t}{\Omega_a} - \frac{X_{tv}}{\tau_t} - \frac{D_v X_v 4\pi r_t X_{tv}}{\Omega_a} = 0 \tag{2b}$$

$$\tau_t \approx \frac{b^2}{[D_v \exp(-H_b/RT)} \tag{2c}$$

Here, r_t ($\approx r_v = 0.57\,nm$) is the trap capture radius, τ_t is the average trapping time, H_b is the trap-vacancy binding enthalpy and b ($=0.248\,nm$) is the atomic spacing. Solute vacancy binding energies are typically in the range of about 5 to $30\,kJ\,mol^{-1}$ [20]. However, the effective H_b may be even higher. Equations (2) can be solved for the ϕ corresponding to a specified $g_{st}(\phi, T_i, S_t, X_t, H_b)$ as

$$\phi(g_{st}) = \frac{(1/g_{st} - 1)S_t/\xi\sigma_{dpa}}{(4\pi r_t \tau_t/\Omega_a(4\pi r_t X_t g_{st}/\Omega_a S_t + g_{st} - 1)) - (4\pi r_v/D_v S_t \Omega_a)} \tag{2d}$$

Recombination can also occur at multiple vacancy trapping sites, including at coherent precipitate interfaces. Trapping at small solute cluster complexes may be particularly important, since the binding energies of additional vacancies are relatively large. For example, assuming the vacancy formation energy is $175\,kJ\,mol^{-1}$ and the surface energy is $1.5\,J\,m^{-2}$, the binding energy for a 5-vacancy cluster is about $70\,kJ\,mol^{-1}$. These (and other) effects can be treated by more detailed rate theory models, but again they can also be accounted for approximately by treating H_b, S_d and X_t as 'effective' parameters. Recombination also occurs at the thermally unstable vacancy cluster complex UMF sinks formed in aged displacement cascades. The UMF build-up to a steady-state concentration and an S_c that is directly proportional to the DR [3, 12] and decreases with increasing T_i. As shown elsewhere [5], it is also possible to account for the UMF sinks by taking $S_t = S_d + S_c$, where S_c is

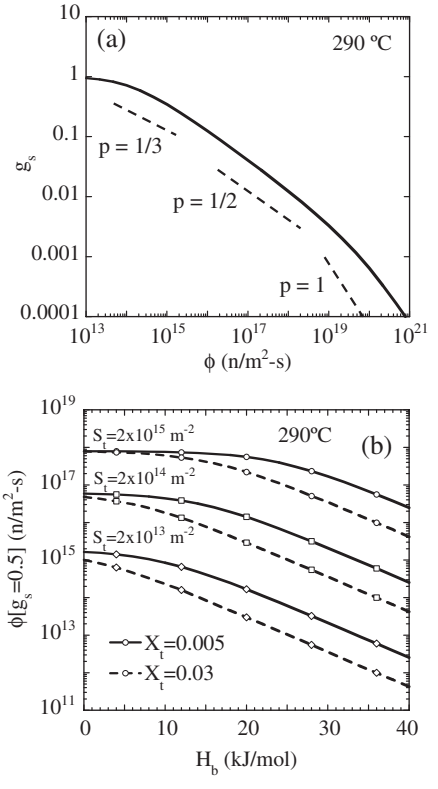

Figure 2. (a) The $g_s(\phi)$ at 290°C showing the transition from sink, to solute trap recombination, to UMF dominance of the fate of vacancies with increasing DR for the nominal parameters given in the text. (b) The ϕ at $g_s = 0.5$ as a function of H_b for various S_d and X_t.

determined from the characteristic UMF annealing time τ_c ($= 3 \times 10^5$ s at 290°C), radius r_c and formation cross section, σ_c ($= 1.5 \times 10^{-29}$ m^2).

Figure 2a plots the $g_s(\phi)$ for $X_t = 0.03$ and $H_b = 30$ kJ mol^{-1}, accounting for all the processes described above, except thermal Cu diffusion, using the nominal model parameters. The g_s transitions between a DR independent, sink dominated regime at very low ϕ, through a solute trap recombination dominated DR regime at intermediate ϕ, to a cascade cluster dominated DR regime at very high ϕ. Figure 2b plots the corresponding ϕ at $g_s = 0.5$ as a function of H_b for various S_d and X_t. These results clearly indicate that solute enhanced recombination is likely to be important over a wide range of DR pertinent to RPV embrittlement.

The RED D* for Cu can be generally expressed as [5]

$$D^* \approx [D_v X_v]\left(\frac{D_{cu}}{D_{sd}}\right) + D_{cu} \approx \left(\frac{g_s \xi \sigma_{dpa} \phi}{S_t}\right)\left(\frac{D_{cu}}{D_{sd}}\right) + D_{cu} \approx K(\phi, T)\phi + D_{cu}. \quad (3a)$$

Here D_{cu}/D_{sd} (>1) is the ratio of the thermal Cu to Fe self-diffusion coefficients, where the RED self-diffusion coefficient is $D^*_{sd} \approx D_V X_V$. The $K(\phi, T)$ is the RED factor, where $D^* = K(\phi, T)\phi$ and

$$K(\phi, T) = g_s\left[\frac{D_{cu}}{D_{sd}}\right]\left[\frac{\xi \sigma_{dpa}}{S_t}\right] \quad (3b)$$

For $D^* \gg D_{cu}$, the maximum RED factor $K_m \neq f(\phi)$ is obtained for $g_s = 1$. A lower-bound empirical extrapolated estimate of $D_s(0.27\%\ Cu)/D_{sd} \approx 5$ at 290°C [21] yields $K_m \approx 1.5 \times 10^{-39}\,m^4$. Fits to the $\Delta\sigma_y(\phi t)$ data (see below) suggest this D* estimate may be low by factors of up to about 60 or more for Ni-bearing alloys. Such differences can be attributed to a combination of underestimates of D_{cu}/D_{sd}, arising from strong solute–vacancy interactions; and, perhaps, overestimates of the dislocation sink strength, S_d. Other effects, such as small mobile vacancy cluster complexes and complex correlated diffusion in semi-concentrated alloys, may also lead to higher effective D* and K_m.

In the recombination-dominated regime, the effect of DR can be described by a simple scaling law as $K(\phi_r) = K(\phi_r)(\phi_r/\phi)^{1/2}$, where ϕ_r is a reference flux ϕ, taken here as $3 \times 10^{15}\,nm^{-2}\,s^{-1}$. More generally $g_s(\phi)/g_s(\phi_r) \approx (\phi_r/\phi)^p$. The p can be evaluated at ϕ_r, or considered to be an effective average for the range of DRs encountered. The DR scaling exponent p varies continuously with increasing ϕ. The effective p starts at 1 in the thermal diffusion dominated regime at very low DR; p is 0 in the sink-dominated regime and $p = 1/2$ in the recombination-dominated regime. The p again approaches 1 at high DRs in the UMF sink-dominated regime. At around 300°C and less $D^* \gg D_{cu}$ at all but the lowest DRs ($\ll 10^{14}\,nm^{-2}\,s^{-1}$). Note, D* also depends on T_i, due to its effect on $X_v(\phi)$ and g_s, as well as the vacancy concentrations and jump rates near a solute atom that control D_{cu}/D_{sd} and D_{cu}. Even if $g_s \ll 1$, deep in the recombination dominated regime, large D* are consistent with strong solute–vacancy binding and correspondingly high values of $[D_{cu}/D_{sd}]$.

We use a generalized Avrami type form [25] to model $f_p(\phi t_e)/f_{pm}$ as a function of the effective fluence (ϕt_e) as

$$\frac{f_p(\phi t_e)}{f_{pm}} = \{1 - \exp[-(F\phi t_e)^{\beta}]\}. \tag{4a}$$

Here, F and β are fit parameters that set ϕt_e scale and interval for precipitation, respectively. Larger *F* means precipitation and hardening occurs at lower ϕt_e. Larger β narrows the ϕt_e region between the start and completion (e.g. 5–95%) of precipitation.

The corresponding $\Delta\sigma_{yp}(\phi t_e)$ is given by

$$\Delta\sigma_{yp}(\phi t_e) = \Delta\sigma_{ypm}\sqrt{\frac{f_p(\phi t_e)}{f_{pm}}}. \tag{4b}$$

Here $\Delta\sigma_{ypm}$ is the plateau CRP hardening fit parameter. If the kinetics are primarily controlled by long-range Cu diffusion to a fixed number (N_p) of growing CRPs, $\beta = 3/2$ [3, 5, 12, 24]. The F can be interpreted as

$$F = (10.55N_p)^{2/3}(X_c/X_p)^{1/3}K(\phi_r). \tag{4c}$$

Here X_e is the Cu initially in solution, X_p is the fraction of Cu in CRPs that are alloyed with Mn and Ni, and $K(\phi_r)$ is the RED factor at the reference ϕ_r. Assuming negligible Cu solubility in ferrite and approximately full precipitation, $f_{pm} \approx X_e/X_p$. The model does not treat precipitate nucleation or coarsening stages, and ignores the modest solubility of Cu in local equilibrium with CRPs. However, assuming $\beta = 3/2$ is based on rather severe approximations of the physics governing precipitation and hardening under irradiation. For example, it is well established that Cu precipitation kinetics involve overlapping regimes of nucleation, growth and coarsening that are

not reflected in the simple diffusion-controlled growth model [3, 12]. And $K(\phi_r)$ may decrease with increasing ϕt due to the build-up of SMF defect sinks. Further, equation (4b) does not fully account for the fact that, in addition to $\sqrt{f_p}$, $\Delta\sigma_{yp}$ also depends on the size, composition and structure of the CRPs. The net $\Delta\sigma_{yp}$ also depends on how the individual CRP contribution combines, or superimposes, with that due to pre-existing obstacles to dislocation slip [3].

The expressions above model $\Delta\sigma_{yp}(\phi t_e)$ as a function of the effective fluence, ϕt_e, and do not depend on DR. The DR dependence is accounted for by adjusting the actual fluence, ϕt, to the effective fluence, ϕt_e, as

$$\phi t_e = \phi t\left(\frac{g_s(\phi, L)}{g_s(\phi_r, L)}\right) = \phi t\left[\frac{g_s(\eta_L)}{g_s(\eta_{Lr})}\right] \tag{4d}$$

Here L is a fit parameter defined by $\eta_L = L\eta$ (or $L\phi$) where g_s and η are given by equations (1b) and (1c). The parameter L sets the scale for recombination. Large L and η_L correspond to a low g_s and a p approaching the recombination-dominated limit of 1/2.

If N_p, X_c and X_p are known, the RED factor $K(\phi_r)$ can be evaluated from equation 4c. The corresponding maximum K without recombination (K_m) at $g_s = 1$ is

$$K_m = \frac{K(\phi_r)}{g_s(L\phi_r)} \tag{4e}$$

A least square procedure was used to optimize the fit parameters F, β, L, $\Delta\sigma_{ypm}$ for each individual alloy irradiated in this study. The DR effect is determined by finding the L that provides the best common $\Delta\sigma_{yp}(\phi t_e)$ fit for the datasets in the low, intermediate and high DR regimes. Since ϕ_r is at the intermediate DR, the $\phi t_e/\phi t$ is >1 for the low DR data and <1 for the high DR data.

4. Results and analysis

Equation (4) was used to analyse the very large IVAR 290°C $\Delta\sigma_y$ database. This database includes a total of 35 Cu-bearing alloys. We have corresponding microstructural information from SANS to provide estimates $K(\phi_r)$ and K_m for a subset of 19 of these alloys. The CRP hardening, $\Delta\sigma_{yp}$, is experimentally defined by subtracting the SMF hardening from the measured $\Delta\sigma_y$ in the Cu-bearing alloys as

$$\Delta\sigma_{yp} = \Delta\sigma_y - B\sqrt{\phi t}. \tag{5a}$$

Here B was found, when possible, by fitting the $\Delta\sigma_y(\phi t)$ data for a steel with the same nominal composition as the particular Cu-bearing alloy being analysed, except that it does not contain Cu. For example, alloy CM3 (0% Cu, 0.8% Ni, 1.6% Mn, 0.005% P) is the no-Cu analogue of the Cu-bearing CM11, 13, 16 and 19 alloys (also with 0.8% Ni, 1.6% Mn, 0.005% P) containing 0.1–0.4% Cu. In cases where the Cu free steel data are not available (like the CWP series alloys), the best fit for a linear function of composition to the individual B for all the low Cu ($<0.1\%$) steels was found to be

$$B = 681P + 460Cu + 10.4Ni + 10.7Mn - 10(MPa). \tag{5b}$$

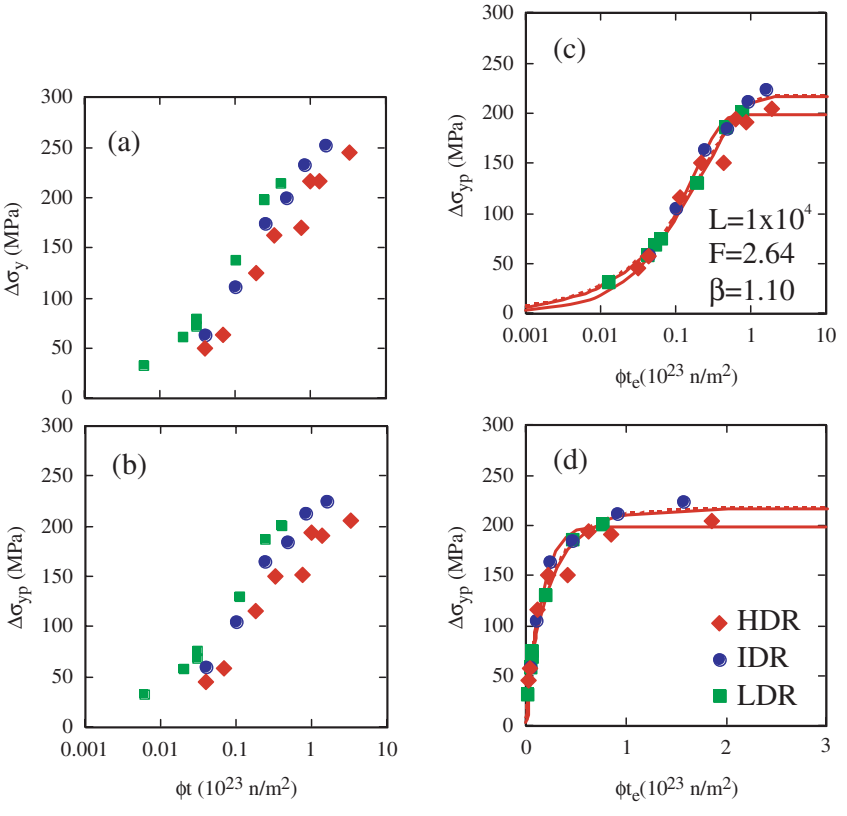

Figure 3. Data trends and analysis of a 0.4% Cu, 1.25% Ni alloy (LD): (a) $\Delta\sigma_y$ versus log ϕt; (b) $\Delta\sigma_{yp}$ versus log ϕt; (c) $\Delta\sigma_{yp}$ versus log ϕt_e; and (d) $\Delta\sigma_{yp}$ versus ϕt_e. The Avrami-type transformation fits for diffusion controlled growth (solid lines) and the generalized β-model (dashed lines) are also shown in (c) and (d).

The resulting B(Cu = 0, Ni, Mn, P) from equation (5b) was then used in equation (5a) to evaluate the $\Delta\sigma_{yp}$ for the particular Cu bearing alloy with a specified Ni, Mn and P content. Since $B\sqrt{\phi t}$ is generally fairly small, the overall uncertainty in evaluating $\Delta\sigma_{yp}$ with these procedures is estimated to be about $\pm$ 15 MPa, which is similar to other sources of experimental scatter in the data.

Figure 3 illustrates the common trends observed in the IVAR database and the results of the fitting procedure. Figure 3a plots the raw $\Delta\sigma_y$ versus logϕt data at low (squares), intermediate (circles) and high (diamonds) DRs for a 0.4% Cu, 1.25% Ni alloy (LD). Figure 3b shows a similar plot for $\Delta\sigma_{yp}$. Both figures 3a and b show that higher DRs shift the $\Delta\sigma_y$ and $\Delta\sigma_{yp}$ to higher ϕt. Figure 3c shows the corresponding plot of the $\Delta\sigma_{yp}$ versus logϕt_e data based on fitting L and β. The solid and dashed curves show the results of fixed $\beta = 3/2$ and fitted β, respectively. As expected, the latter generally results in a slightly better fit. Notably, the $\Delta\sigma_{yp}$ fall in a common band when plotted on the logϕt_e scale. In this case, the g_s are 0.023, 0.036 and 0.069 for the high, intermediate and low DRs respectively, corresponding to an average $p \approx 0.49$, essentially at the recombination dominated limit. These results clearly indicate that a large amount of recombination occurs in this alloy even at the lowest DR. Figure 3c also shows the $\Delta\sigma_{yp}$ plateaus at $\Delta\sigma_{ypm}$ at high ϕt_e. This is more clearly seen in figure 3d showing a linear plot of $\Delta\sigma_{yp}$ versus ϕt_e.

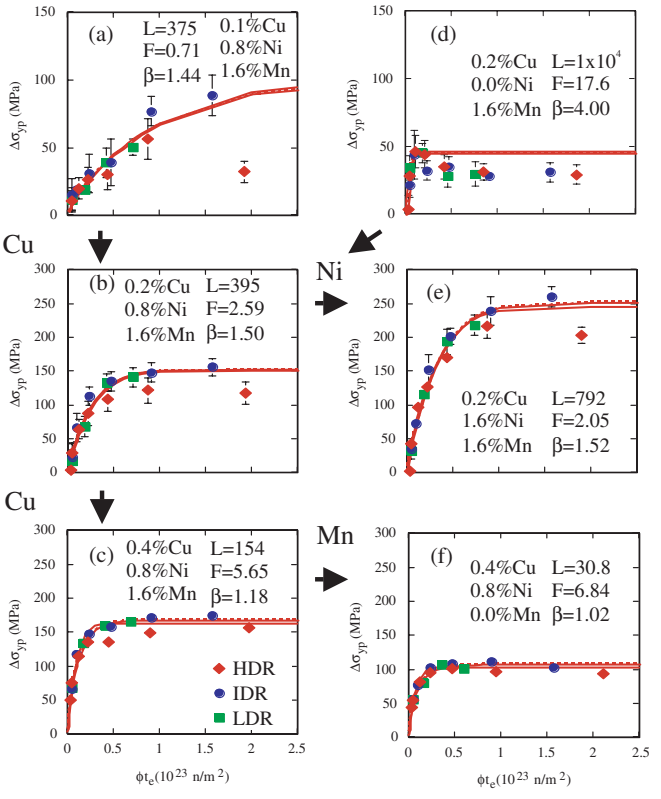

Figure 4. Effects of Cu, Ni and Mn variation on the $\Delta\sigma_{yp}(\phi t_e)$ along with the diffusion controlled growth (solid lines) and generalized (dashed lines) Avrami-type model fits.

Figure 4 shows plots of $\Delta\sigma_{yp}$ versus $\log\phi t_e$ for a series of CM alloys with different Cu, Ni and Mn contents. The narrow pre-plateau trend band of $\Delta\sigma_{yp}(\phi t_e)$ data at the various DRs is similar to that shown in figure 3c. However, in some cases the high DR plateau $\Delta\sigma_{ypm}$ falls somewhat below, and in one case significantly below, the corresponding intermediate and low DR data. Further, the 0.2% Cu alloy without Ni shows an over-aging type decrease in $\Delta\sigma_{yp}$, following a peak at a relatively low ϕt_e. The $\Delta\sigma_{yp}$ are small for both the low 0.1% Cu and 0.0% Ni free alloys. The $\Delta\sigma_{ypm}$ are much larger for alloys with a significant Cu, Ni and Mn content. Clearly, higher Ni and, to a lesser extent, higher Mn result in a very large increase in $\Delta\sigma_{ypm}$ (note the change in scale). These elements also affect the pre-plateau ϕt_e dependence of $\Delta\sigma_{yp}$. Lower Cu and higher Ni and Mn shift the $\Delta\sigma_{yp}$-curves to higher ϕt_e. These specific examples are completely representative of the behaviour of essentially all other alloys in the IVAR database [5].

Indeed, the IVAR database is an enormously rich source of information on both the individual and combined effects of essentially all the significant irradiation and material variables on irradiation hardening. More detailed and comprehensive analysis of this database is given elsewhere [5], and will be the subject of future publications. The focus of this paper is on DR effects at 290°C. However, the trends in the overall IVAR database can be summarized briefly as follows:

- For a specified alloy and T_i (= 290 and 270°C), DR effects in the pre-plateau region can be accounted for by adjusting the actual ϕt to an effective $\phi t_e \approx \phi t(\phi_r/\phi)^{1/2}$ based on a simple rate theory model and fit parameter that sets the scale of recombination. DR effect is not observed at $T_i = 310$°C.
- The plateau $\Delta\sigma_{ypm}$ is independent of DR at low and intermediate ϕ, but is lower in some cases at high ϕ.
- Avrami-type precipitation hardening models provide good fits to the $\Delta\sigma_{yp}(\phi t_e)$ data.
- Lower Cu increases the minimum ϕt_e for the initiation of hardening and $\Delta\sigma_{yp}$ is ≈ 0 for Cu < 0.1%. Variations in Ni do not affect significantly the threshold ϕt_e marking the start of CRP hardening. However, higher Ni increases the ϕt_e needed to reach the plateau $\Delta\sigma_{ypm}$. There is an indication of decreases (over-ageing) in $\Delta\sigma_{yp}$ at high ϕt_e in some alloys that do not contain Ni.
- Higher Ni increases $\Delta\sigma_y$, $\Delta\sigma_{yp}$ and $\Delta\sigma_{ypm}$; and Mn has a similar, but smaller, effect.

We will focus here on further quantifying DR effects using the generalized Avrami model, since it provides a slightly better fit to the $\Delta\sigma_{yp}(\phi t_e)$ data; however, the trends for the diffusion-controlled growth model ($\beta = 3/2$) are generally very similar. With the exception of two CM-series alloys with no Ni, the averaged β is $\approx 1.2 \pm 0.25$. The β was ≈ 4 for the two CM alloys with 0.0% Ni; this indicates a very narrow ϕt_e range for hardening between the threshold and plateau limits.

Figure 5a plots the average DR scaling exponent p versus Ni for various alloy groupings indicated in the legend and described below. Averaging mitigates the large scatter in the results for individual alloys. In great part, this scatter arises from the relative insensitivity of the statistical fits to the precise value of p, especially deeper in the recombination regime (at p values approaching the limiting value of 1/2), as well as other limitations in some subsets of the data. For example, in low Ni alloys there is little $\Delta\sigma_{yp}$ data in the pre-plateau region to fit. The filled circles are for the CM, L and CWP-series with >0.1% Cu and >1.2% Mn. The overall average p is $\approx 0.38 \pm 0.12$. The p for two lower Mn alloys (one with 0% Mn and the other with $\approx$0.8% Mn, open circles) with $\approx$0.8% Ni was lower, averaging $p \approx 0.34$. The p for two other alloys with a much higher bulk 0.8% Cu content (filled diamond) or higher final heat treatment temperature of 664 versus 600°C (open triangle), were

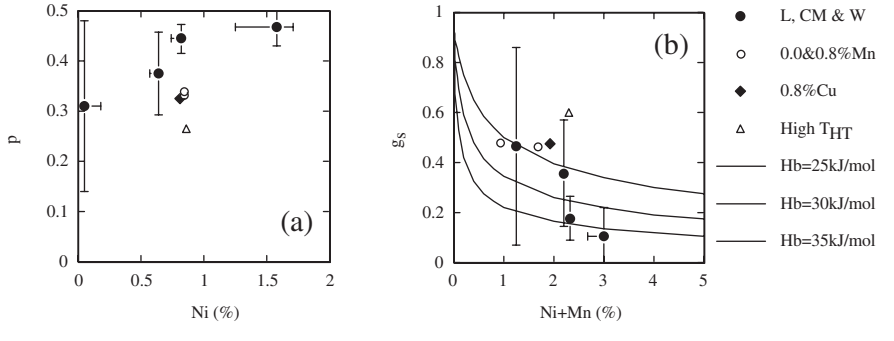

Figure 5. (a) Variation in the experimentally estimated DR scaling exponent, p, with Ni. (b) The observed variation of the experimentally estimated $g_s(\phi_r)$ with the solute vacancy trap concentration taken as $X_t = Ni + Mn$, and the corresponding predictions of the rate theory model using the nominal parameters for $H_b = 25$ to 35 kJ mol^{-1}.

also somewhat lower, averaging $p \approx 0.3$. The average p for all the other CM, L and CWP-series alloys increased with increasing Ni, approaching the recombination limit of 1/2: $p \approx 0.31$ for $\leq$0.3% Ni; $p \approx 0.38$ for $\approx$0.6% Ni; $p \approx 0.45$ for 0.8% Ni; and $p \approx 0.47$ for $\geq$1.2% Ni.

The corresponding overall average for $g_s(\phi_r)$ was $\approx 0.32 \pm 0.26$. The average $g_s(\phi_r)$ for the two lower Mn alloys was 0.47 and was 0.53 for the high 0.8% Cu steel and for the alloy with 664°C heat treatment. The averaged $g_s(\phi_r)$ decreases (recombination increases) with increasing Ni content: $g_s(\phi_r) \approx 0.46$ for $\leq$0.3% Ni; $g_s(\phi_r) \approx 0.35$ for $\approx$0.6% Ni; $g_s(\phi_r) \approx 0.18$ for 0.8% Ni; and $g_s(\phi_r) \approx 0.11$ for $\geq$1.2% Ni. The average $g_s(\phi_r)$ data are shown in figure 5b plotted against the total alloy Mn + Ni solute concentration. These data are in reasonable agreement with the vacancy trap recombination model predictions of g_s versus X_t (= Mn + Ni) also shown for H_b from 25 to 35 kJ mol^{-1} as the solid and dashed lines.

The specified form of the recombination expression given in equation (1) also provides a quantitative basis to extrapolate the results of this study to lower DRs. Such extrapolation can be used to address the question: what is the low ϕ bound (ϕ_{dr}) of the DR-dependent regime due to recombination? Of course ϕ_{dr} depends on the recombination criterion used; a reasonable choice is less than 20% recombination, or a $g_s \geq 0.8$. Figure 6a plots $\phi_{dr}(g_s = 0.8)$ versus Ni. While the points are very scattered, and have large individual error bars, an overall trend to decreasing ϕ_{dr} with increasing Ni is clearly evident. Except for some cases at low or no Ni, the ϕ_{dr} is below, and at higher Ni levels significantly below, $\phi = 10^{15}$ nm^{-2}s^{-1}. These results explain why the embrittlement rates observed in very low DR Boiling Water Reactor (BWR) surveillance programs are higher than found for PWRs at a factor of $\approx$20 times higher DRs. Note that the ϕ_{dr} boundary for recombination does not preclude contributions of anomalous thermal Cu diffusion to an additional DR effect at even lower ϕ as illustrated in figure 1b.

Another pertinent question is — assuming there is a DR effect what is its significance and consistency for various steels and irradiation conditions? Of course the answer to this question is that it depends of the specific alloy Cu, Ni and Mn composition, T_i and ϕt. However, the significance and consistency of DR to the data in the IVAR 290°C database, spanning about a factor of 10 in ϕ, is shown in figure 6b. Here the predicted values of $\triangle\sigma_{yp}$ for irradiations at the intermediate DR reference ϕ_r, for all the individual alloy fits, are plotted against the corresponding actual measured values. Thus, if there were no DR effects, the data would all fall in the same scatter band. However, the least square fit lines show that the low DR results in $\Delta\sigma_{yp}$ that are on average $\approx$ 50% larger than for the high DR irradiations. Considering the modest range of φ, the DR effect is obviously very significant.

The fit parameters can also be used in equations (4c) and (4e) to estimate RED diffusion factors $K(\phi_r)$ and K_m based on SANS measurements of the nominal N_p, X_c and X_p that are summarized elsewhere [5]. Figure 7a shows that $K(\phi_r)$ (equation (4c)) decreases systematically with increasing Ni. Considering alloys with more than 1.2% Mn, the $K(\phi_r)$ for the steel with 0.0% Ni is 2.3×10^{-37} m^4; the corresponding average is $\approx 1.24 \times 10^{-38}$ m^4 for the CM and L-series plates and welds with $\approx$0.6–0.8% Ni and $\approx 2.9 \times 10^{-39}$ m^4 for the CM-series plates and welds with $>$1.2% Ni. The decrease in $K(\phi_r)$ with increasing Ni is partially due to the corresponding increase in solute trap recombination and the corresponding decrease in g_s. Figure 7b shows that the maximum RED factor, K_m (equation (4e)), without recombination, also decreases with increasing Ni, but by a much smaller amount.

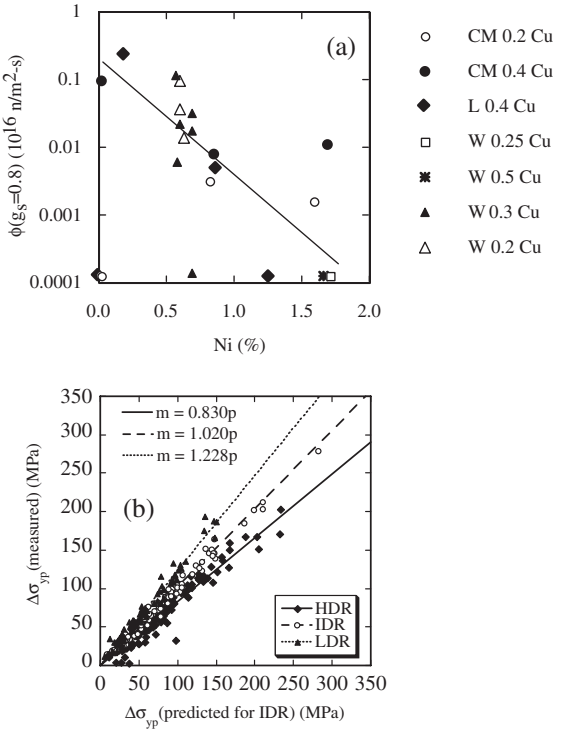

Figure 6. (a) Variation in the experimentally estimated RED factor $K(\phi_r)$ with Ni at the reference DR. (b) Variation of the experimentally estimated maximum K_m with Ni compared to the simple rate theory estimate (dashed horizontal line).

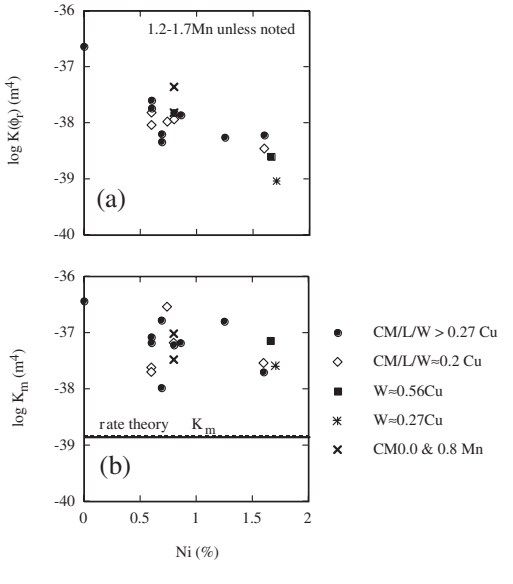

Figure 7. (a) Variations in the $\phi_{dr}(g_s = 0.8)$ with Ni, marking an effective lower limit on the DR dependent ϕ-regime based on extrapolation using the solute trap recombination model. (b) The predicted $\Delta\sigma_{yp}$ at the reference ϕ_r versus the actual measured values at low, intermediate ($\phi \approx \phi_r$) and high DRs.

The even larger scatter band ($\approx$ a factor of 10) for the K_m estimates is primarily due to the uncertainties in g_s. The K_m is $\approx 3.8 \times 10^{-37}\,m^4$ for the 0.0% Ni alloy. The corresponding averages are $K_m \approx 8.0 \times 10^{-38}\,m^4$ for the alloys with $\approx$0.6–0.8% Ni and $K_m \approx 4.4 \times 10^{-38}\,m^4$ for the alloys with $>$1.2% Ni. Notably, these K_m fall well above the simple rate theory model estimate of $\approx 1.5 \times 10^{-39}\,cm^4$. For the Ni-bearing alloys, the average difference ranges between a factor of $\approx$30 to 60 or more. Thus these results show that RED of Cu (and other solutes) is very efficient even when there is a significant amount of solute trap recombination that gives rise to a strong DR effect.

The very high efficiency of excess vacancies produced by irradiation in accelerating solute diffusion is not fully understood. However, as noted previously, this is probably due to a combination of mechanisms, including the rapid diffusion of small vacancy cluster–solute complexes, correlated diffusion processes that occur at low temperature in semi-dilute alloys with strong vacancy–solute (e.g. Cu, Mn, Ni, etc.) interactions and effective defect sink strengths that are smaller than the actual dislocation density used in the rate theory model. Notably, the large values of K_m also imply a large D_{cu}/D_{sd}, hence, high thermal D_{cu} at low temperature. This is also consistent with the unexpectedly rapid thermal age hardening at low temperatures due to precipitation of Cu.

5. Summary and conclusions

The results of this study provide a robust basis to assess DR effects on 290°C hardening and embrittlement of RPV steels.

1. The pre-plateau CRP contribution to hardening, $\Delta\sigma_{yp}(\phi t)$, is shifted to higher ϕt with increasing DR. The shift can be accounted for by normalizing the data to an effective fluence, $\phi t_e \approx \phi t(\phi_r/\phi)^p$. The average p for the IVAR database is $\approx$0.4, indicating that recombination is responsible for the DR effect in the ϕ regime encompassed by the IVAR experiment.
2. The IVAR database shows that, on average, $\Delta\sigma_{yp}$ is about 50% higher at the low compared to high DR, spanning about a factor of 10 in ϕ.
3. The effect of DR increases with increasing alloy solute content, approaching the recombination dominated limit of $p = 1/2$ at high Ni and Mn levels. It is estimated that between 60 and 90% (or more) of the vacancies and SIA recombine at the reference DR of $\phi_r = 3 \times 10^{15}\,n\,m^{-2}$-s. These observations provide strong support for the hypotheses that DR effects primarily arise from a solute vacancy trap enhanced recombination mechanism. The *effective* solute (Mn and Ni)-vacancy binding energy is estimated to be in the range of $\approx 30\,kJ\,mol^{-1}$.
4. The estimated lower bound ϕ_{dr} for the recombination DR regime is les than to much less than $\approx 2 \times 10^{14}\,nm^{-2}$ for RPV alloys with typical contents of 0.6–0.8% Ni; and ϕ_{dr} is even lower for higher Ni levels. A DR-dependent regime may also occur at even lower ϕ due to thermal diffusion of Cu.
5. The plateau $\Delta\sigma_{ypm}$ is independent of ϕ at low and intermediate DR but, in some cases, is somewhat lower at the highest DR.
6. In spite of the large amount of recombination, RED is extremely efficient. Estimates of the maximum RED factor, K_m, for Ni-bearing alloys range from

about 30 to 60 or more times higher than predicted by simple rate theory estimates.

7. There are a number of possible explanations of the high RED efficiency including: (a) lower effective defect sink strengths than that based on the estimated total dislocation density; (b) rapid diffusion of small vacancy cluster-solute complexes; (c) correlated diffusion processes in semi-dilute alloys; and (d) strong vacancy–solute binding interactions, that not only increase recombination, but also significantly influence the jump frequencies of vacancies in the vicinity of solutes, resulting in $D_{cu} \gg D_{sd}$. Such solute–vacancy interaction effects are also consistent with the anomalously high values of low temperature thermal diffusion effects discussed in section 1.

Finally, we note that the results of this study are generally consistent with a similar analysis of SANS data on the CRP evolutions that will be reported in the future.

Acknowledgements

The authors gratefully acknowledge the many people who have contributed to the UCSB IVAR program. Phil Simpson (University of Michigan) and Dennis Heatherly (ORNL) have been instrumental in making IVAR facility a great success. We thank David Gragg (UCSB) for his tireless contributions to the preparation of the specimens and irradiation capsules. We also appreciate many helpful discussions with our colleagues Brian Wirth (UC Berkeley), Gene Lucas (UCSB), Tim Williams (RRA), Randy Nanstad (ORNL) and Colin English (AEA Harwell), and also thank them for other contributions too numerous to list. The sets of alloys supplied by Wayne Pavanich (consultant), Randy Nanstad, Tim Williams and P. Tipping (Paul Scherrer Institute) were also a key element of this work. This research was funded under NRC Contracts #04-94-049 and 04-01-064. Thus we also express thanks to our NRC program monitors, Mike Vassilaros, Carolyn Fairbanks and Tanny Santos, for providing continuing encouragement and support. Finally, although not the focus of the present paper, we also acknowledge the outstanding facilities and staff at the NIST Center for Neutron Research, where we carried out our SANS measurements.

References

[1] G.R. Odette and G.E. Lucas, *Irradiation Embrittlement of Reactor Pressure Vessel Steels*, EPRI NP 6114 (1989).
[2] E.D. Eason, J.E. Wright and G.R. Odette, *Improved Embrittlement Correlations for Reactor Pressure Vessel Steels*, NUREG/CR-6551 (U.S. Nuclear Regulatory Commission, Washington, DC, 1998).
[3] G.R. Odette and G.E. Lucas, Radiat. Eff. Def. Solids **144** 189 (1998).
[4] G.R. Odette, G.E. Lucas, D. Klingensmith *et al.*, *The Effects of Composition and Heat Treatment on Hardening and Embrittlement of Reactor Pressure Vessel Steels*, NUREG/CR-6778 (U.S. Nuclear Regulatory Commission, Washington, DC, 2003).
[5] G.R. Odette, T. Yamamoto, D. Klingensmith *et al.*, *The Effect of Flux and Irradiation, Temperature on Hardening in RPV Steels*, UCSB-NRC-LR-03/2 (2003).
[6] G.R. Odette, Scripta Met. **11** 1183 (1983).
[7] S.B. Fisher and J.T. Buswell, Int. J. Pressure Vessels Piping **27** 91 (1988).
[8] G.R. Odette, B.D. Wirth, D.J. Bacon *et al.*, MRS Bull. **26** 176 (2001).

[9] T.J. Williams and D. Ellis, in *Effects of Radiation on Materials: 20th International Symposium*, ASTM STP 1405, edited by S.T. Rosinski *et al.* (American Society for Testing and Materials, West Conshohocken, PA, 2001), pp. 8–27.
[10] R.G. Carter, N. Soneda, *Workshop on Dose Rate Effects in Reactor Pressure Vessel Materials*, Electric Power Research Institute Conference Proceedings, EPRI 1006981 (2002) (CD).
[11] G.R. Odette, E.V. Mader, G.E. Lucas *et al.*, in *Effects of Radiation on Materials — 17th International Symposium*, ASTM-STP 1175, edited by A.S. Kumar *et al.* (American Society for Testing and Materials, West Conshohocken, PA, 1993), pp. 373–393.
[12] G.R. Odette, in *Irradiation Effects on Pressure Vessel Steels*, IAEA IRRWG-LMNPP-98-3 (International Atomic Energy Agency, Vienna, Austria, 1998), pp. 438–504.
[13] B.D. Wirth, G.R. Odette and R.E. Stoller, *Multiscale Modeling of Materials*, MRS Soc. Symp. Proc. 677, edited by V. Bulatov *et al.* (Materials Research Society, Warrendale, PA, 2001), AA5.2.
[14] G.R. Odette, G.E. Lucas and D. Klingensmith, in *Effects of Radiation on Materials, 18th International Symposium*, ASTM-STP 1325, edited by R.K. Nanstad *et al.* (American Society for Testing and Materials, West Conshohocken, PA, 1999), pp. 88–101.
[15] M.K. Miller, K.F. Russell, G.R. Odette *et al.*, *Precipitation in Thermally Aged and Neutron Irradiated Fe–Cu and Fe–Cu–Mn Model Alloys*, ORNL/NRC/LTR-03/01 (2003).
[16] G.R. Odette and C. Cowan, in *Proceedings of the 10th International Symposium on Environmental Degradation of Materials in Light Water Reactors*, edited by G.S. Was and J.L. Nelson (NACE, 2001) (CD).
[17] B.D. Wirth, G.R. Odette, P. Asoka-Kumar *et al.*, *Proceedings of the 10th International Symposium on Environmental Degradation of Materials in Light Water Reactors*, edited by G.S. Was and J.L. Nelson (NACE, 2001) (CD).
[18] M.K. Miller, B.D. Wirth and G.R. Odette, Mater. Sci. Eng. A **353** 133 (2003).
[19] E. Mader, Kinetics of irradiation and the post-irradiation annealing of nuclear reactor pressure vessel steels. Ph.D. thesis, University of California, Santa Barbara (1995).
[20] A. Moeslang, E. Albert, E. Recknagel *et al.*, *Hyperfine Interact*. **15/16** 409 (1983).
[21] G. Salje and M. Feller-Kneipmeier, J. Appl. Phys. **48** 1833 (1977).
[22] J. Marian, B.D. Wirth, J.M. Perlado *et al.*, *Microstructure in Irradiated Materials — 2000*, MRS Symp. Proc. 650 (Materials Research Society, Warrendale, PA, 2001), R6.9.
[23] A.D. ???, Phil. Mag. **972** 819 (1970).
[24] I. Remic, C.A. Baldwin and E.D. Blakeman, *Characterization of the Neutron Field in the HSSI/UCSB Irradiation Facility at the Ford Nuclear Reactor*, NUREG/CR-6646 (1999).
[25] E.S. Machlin, *An Introduction to Thermodynamics and Kinetics Relevant to Materials Science*, 2nd edition (Giro Press, Croton-on Hudson, NY, 1999).
[26] L.K. Mansur, A.D. Brailsford and W.G. Wolfer, J. Nucl. Mater. **105** 36 (1982).
[27] B.N. Singh, S.I. Golubov, H. Trinkaus *et al.*, J. Nucl. Mater. **251** 107 (1997).
[28] R.E. Stoller, *Effects of Radiation on Materials, 18th International Symposium*, ASTM-STP 1325, edited by R.K. Nanstad *et al.* (American Society for Testing and Materials, West Conshohocken, PA, 1999) pp. 14–29.